HHS Public Access

Author manuscript

Hear Res. Author manuscript; available in PMC 2017 September 01.

Published in final edited form as:

Hear Res. 2016 September ; 339: 50–59. doi:10.1016/j.heares.2016.05.016.

Membrane Prestin Expression Correlates with the Magnitude of Prestin-Associated Charge Movement

Michelle L. Seymour[a,*], **Lavanya Rajagopalan**[b,d,*], **Guillaume Duret**[e], **Matthew J. Volk**[b], **Haiying Liu**[a], **William E. Brownell**[b,c], and **Fred A. Pereira**[a,b]

Michelle L. Seymour: mlseymou@bcm.edu; Lavanya Rajagopalan: lavanya.rajagopalan@gmail.com; Guillaume Duret: gd4@rice.edu; Matthew J. Volk: Matthew.Volk@gmail.com; Haiying Liu: haiyingl@bcm.edu; William E. Brownell: brownell@bcm.edu; Fred A. Pereira: fpereira@bcm.edu

[a]Huffington Center on Aging and Department of Molecular and Cellular Biology, Baylor College of Medicine, Houston, Texas 77030, USA

[b]Bobby R. Alford Department of Otolaryngology-Head and Neck Surgery, Baylor College of Medicine, Houston, Texas 77030, USA

[c]Department of Neuroscience, Baylor College of Medicine, Houston, Texas 77030, USA

[d]W. M. Keck Center for Interdisciplinary Bioscience Training, Houston, TX 77005, USA

[e]Department of Bioengineering, Rice University, Houston, TX 77030, USA

Abstract

Full expression of electromotility, generation of non-linear capacitance (NLC), and high-acuity mammalian hearing require prestin function in the lateral wall of cochlear outer hair cells (OHCs). Estimates of the number of prestin molecules in the OHC membrane vary, and a consensus has not emerged about the correlation between prestin expression and prestin-associated charge movement in the OHC. Using an inducible prestin-expressing cell line, we demonstrate that the charge density, but not the voltage at peak capacitance, directly correlates with the amount of prestin in the plasma membrane. This correlation is evident in studies involving a controlled increase of prestin expression with time after induction and inducer dose-response. Conversely, membrane prestin levels and charge density gradually decline together following the reduction of prestin levels from a steady state by removal of the inducer. Thus, charge density directly correlates with the level of membrane prestin expression, whereas changing membrane levels of prestin have no effect on the voltage at peak capacitance in this inducible prestin-expressing cell line.

Keywords

prestin; membrane; charge density; non-linear capacitance

Address Correspondence to: Fred A. Pereira, Baylor College of Medicine, One Baylor Plaza, Houston, TX 77030, Tel.: (713) 798-6933, Fax: (713) 798-1610, fpereira@bcm.edu.

*These authors contributed equally to this work.

Introduction

Prestin is an integral membrane protein that resides in the lateral wall of cochlear outer hair cells (OHCs) and is an essential component of the membrane-based motor that powers electromotility, a central mechanism in mammalian audition (Adler et al., 2003; Belyantseva et al., 2000; Liberman et al., 2002; Mahendrasingam et al., 2010; Yu et al., 2006; Zheng et al., 2000). Prestin, in conjunction with the OHC membrane and other anions, responds to changes in electrical potential across the membrane to generate mechanical motion; this electromechanical transduction process is termed electromotility (Ashmore, 2008; 1987; Brownell, 2006; Brownell et al., 1985; Kalinec et al., 1992; Zheng et al., 2000). OHC electromotility is accompanied by charge movement, which is characterized by a bell-shaped non-linear capacitance (NLC) function (Ashmore, 1990; Ludwig et al., 2001; Oliver et al., 2001; Santos-Sacchi, 1991a; 1991b). The NLC provides a relatively convenient readout of OHC function and is widely regarded as the electrical signature of electromotility.

The requirement of prestin function for full expression of OHC electromotility, generation of NLC and high-acuity mammalian hearing is well-documented. Prestin knockout mice exhibit a 40–60 dB loss of cochlear sensitivity and lack OHC electromotility, NLC, and voltage-dependent stiffness (He et al., 2010; Liberman et al., 2002). However, this mouse model also contains confounding features—shorter OHC length and compromises in mechanical integrity— that complicate isolation of the prestin contribution to electromotility and cochlear amplification (Dallos et al., 2008; Liberman et al., 2002). OHCs from a prestin knockin mouse model with diminished prestin function but preserved mechanical integrity and proper targeting of prestin to the membrane behave similarly to prestin-null OHCs, thus demonstrating that cochlear amplification requires prestin-based electromotility (Dallos et al., 2008). Additionally, prestin-null OHCs transduced to express prestin generate normal NLC profiles (Xia et al., 2008), implicating prestin's sufficiency to generate prestin-associated charge movement in OHCs.

Studies of OHC functional development suggest that the expression and localization of prestin in the OHC membrane coincides with the appearance and maturation of NLC and electromotility (Abe et al., 2007; Belyantseva et al., 2000; Oliver et al., 2001; Zheng et al., 2000). However, a consensus has not emerged about the exact timelines of prestin expression and NLC maturation, which raises questions about the direct correlation between membrane levels of prestin and prestin-associated charge movement. Moreover, many studies investigating prestin-associated charge movement make the fundamental assumption that there is a direct relationship between the molecular density of prestin in the membrane and the amount of charge moved (Abe et al., 2007; Belyantseva et al., 2000; Muallem and Ashmore, 2006; Rybalchenko and Santos-Sacchi, 2008; 2003; Schaechinger and Oliver, 2007). This assumption, however, has not been comprehensively validated. A tetracycline-inducible prestin-expressing cell line has previously been created to model prestin's functional maturation; however, this cell line over-expresses prestin at levels well above those seen with transient transfection methods, and subsequent studies focus primarily on contribution of different prestin oligomeric states to electrical measures of prestin activity (Bian et al., 2010; 2013). To enhance understanding of how prestin expression correlates with NLC parameters, we had created an inducible prestin-expressing cell line in which we

modulate prestin expression by varying both the dosage of an inducer and the time after induction and correlate the prestin-associated charge movement with prestin membrane expression. We also compare the findings from our inducible cell line to NLC parameters from isolated murine outer hair cells (OHCs). Our findings are relevant to OHC development and the factors that influence prestin function.

Materials and Methods

Materials

Pierce Cell Surface Protein Isolation Kit and trichloroacetic acid (TCA) were obtained from Thermo Fisher Scientific (Rockford, IL). Doxycycline, G418 and hygromycin were all purchased from Clontech (Mountain View, CA). Goat polyclonal anti-prestin (N-20) primary antibody (1:250) was purchased from Santa Cruz Biotechnology, Inc. (Santa Cruz, CA), and rabbit monoclonal anti-EGFR primary antibody (1:1000) was purchased from Cell Signaling Technology (Danvers, MA). Odyssey blocking buffer, donkey anti-goat IRdye 800 secondary antibody (1:5000), and goat anti-rabbit IRdye 680 secondary antibody (1:5000) were purchased from LI-COR Biotechnology (Lincoln, NE).

Transient transfection of prestin into HEK 293 cells

Gerbil prestin was cloned into the pIRES-GFP vector as a HA-tag-fusion protein (HA-prestin) as previously described (Rajagopalan et al., 2006; Sturm et al., 2006). HEK 293 cell lines were maintained with Dulbecco's Modified Eagle's Medium (DMEM) with 10% FBS and 1% streptomycin and penicillin. 24h after passage or at ~50% confluence, cells were transfected with WT HA-prestin at a 3:1 ratio with FuGene 6 or X-tremeGENE 9 DNA transfection reagent (both from Roche, Indianapolis, IN). Transfection was verified by the presence of epifluorescence from GFP expressed independently from the same plasmid. Quantification of prestin cell surface expression and electrophysiological measurements were performed between 10 and 48 hours post-transfection.

Construction of Prestin-mGFP Tet-On Inducible System

We used the Tet-On Gene Expression System (Clontech, Mountain View, CA) to create a stable HEK 293 cell line with doxycycline (Dox)-dependent expression of prestin. The Tet-On vector contains a neomycin resistance gene and a reverse Tet repressor gene (rTetR) that codes for the regulatory protein; the response plasmid (TRE2-Tight) contains the Tet response element (TRE), which is regulated by rTetR only upon binding to Dox. First, an HEK 293 cell line stably transfected with the rTetR plasmid was generated by selection with G418. Prestin-mGFP was cloned into the TRE2-Tight plasmid, and co-transfected into the HEK-rTetR stable cell line along with the pTK-Hyg hygromycin selection vector. All transfections were carried out using Fugene 6 (Roche, Indianapolis, IN). After 48 hours, G418 and hygromycin were added and replenished every four days. After two weeks, multiple independent surviving colonies were selected for inducible prestin expression upon administration of Dox. A single colony that showed tightly controlled inducible prestin expression was then expanded and used for all further experiments. Quantification of cell surface protein expression and electrophysiological measurements were performed at i) time points (0, 16, 24, 40, 48, 64, and 72 hours) after induction with 2 μg/ml Dox; ii) at 48 hours

after induction by Dox doses (0, 0.5, 1, 2, 4, 6, 8 or 10 μg/ml); or iii) at specific time points (0, 12, 24, 36, and 48 hours) after Dox removal from cells induced with 2 μg/ml Dox for 48 hours.

Quantification of Prestin Cell Surface Expression

Membrane proteins were isolated from intact cells after surface protein biotinylation using the Pierce Cell Surface Protein Isolation Kit (Thermo Fisher Scientific, Rockford, IL). Briefly, transiently transfected cells or inducible cells treated with 2 μg/ml Dox for different periods, with different doses of Dox for 48 hrs or with removal of Dox at specific time points were incubated with 400 μM membrane-impermeable sulfosuccinimidyl-2-(biotinamido)ethyl-1,3-dithiopropionate for 30 min at 4°C before the reaction was quenched. Cells were then lysed, and Bradford assays were performed to quantify the total protein collected from each of the triplicate dishes of cells for the experiments described above. Equal quantities of biotinylated products were captured on NeutrAvidin-agarose beads and washed. Purified proteins were eluted using a sample buffer containing 50 mM dithiothreitol. Eluted proteins were precipitated with 100% (w/v) trichloroacetic acid, pelleted and resuspended in Laemeli sample buffer (62.5 mM Tris-HCl pH 6.8, 10% glycerol (v/v), 2% sodium dodecyl sulfate (SDS) (w/v), 0.1% (w/v) bromophenol blue). After proteins were denatured at 95°C for 10 minutes, samples were fractionated by 7.5% SDS polyacrylamide gel electrophoresis (SDS-PAGE) and transferred to nitrocellulose membranes. Membranes were blocked with equal volumes of Odyssey blocking buffer and phosphate buffered saline. Membranes were probed with goat anti-prestin (N-20) primary antibody (1:250) followed by donkey anti-goat IRdye 800 secondary antibody (1:3500), imaged, stripped, and reprobed with rabbit anti-EGFR primary antibody (1:1000) followed by goat anti-rabbit IRdye 680 secondary antibody (1:5000) to normalize for equal loading of membrane proteins. Blots were imaged using an Odyssey gel imaging system (LI-COR, Lincoln, NE), and quantification of band pixel intensity was performed with Odyssey 3.0 software and analyzed using R (version 2.13.0) for statistical significance. The Student's t-test with Holm adjustment of p-values for multiple comparisons was used to estimate statistical significance. The Holm method of adjusting p values was used to control the family-wise error rate when making multiple comparisons, which increases statistical power without making dependence assumptions on the data (Holm, 1979).

OHC Isolation

Two-month-old C57BL/6 mice were euthanized by CO_2 asphyxiation, decapitated and cochleae dissected immediately. The cochlea was then separated from the temporal bone in extracellular buffer and cut in half. Each part was individually incubated in 0.5 mg/mL collagenase in extracellular blocking buffer solution (99 mM NaCl, 20 mM TEA-Cl, 2 mM $CoCl_2$, 1.47 mM $MgCl_2$,1 mM $CaCl_2$,10 mM HEPES, titrated to pH 7.2 and osmo-adjusted with dextrose to 300 mOsm for OHCs (Osmette A, Precision Systems, Natick, MA)) for 20 minutes at 37°C to dissociate the cells. The samples were then kept on ice until use. At the time of transfer to the electrophysiology chamber, the OHCs were further dissociated by gentle pipetting. Selected cells had a uniform cylindrical shape with a basally located nucleus. The Baylor College of Medicine and Rice University Institutional Animal Care and Use Committees approved all experiments and procedures using animals.

Electrophysiological measurements

Electrophysiological data were obtained from HEK 293 cells and isolated murine OHCs using the whole-cell voltage clamp technique. Our recording techniques are fully described earlier (McGuire et al., 2010; Rajagopalan et al., 2006), but a brief description follows. Murine OHCs were used within 4 hours of isolation and within 1 hour of being in the recording chamber at RT. All cells retained for analysis exhibited series resistance less than 10 MΩ and membrane resistance in excess of 1 GΩ for HEK 293 cells and 300MΩ for OHCs. Culture dishes containing transfected cells were placed on the stage of an inverted microscope (Carl Zeiss, Gottingen, Germany) under 100X magnification and extensively perfused with the extracellular solution containing Ca^{2+} and K^+ channel blockers (in mM: 100 NaCl, 20 CsCl, 20 tetraethylammonium-Cl, 10 HEPES, 2 $CoCl_2$, 1.47 $MgCl_2$, and 2 $CaCl_2$) prior to recording. All recordings were conducted at room temperature (23°C ± 1°C). The intracellular pressure was controlled with a high-speed pressure clamp (ALA Scientific Instruments, Inc., Farmingdale, NY). Patch pipettes (quartz glass) with resistances ranging from 2 – 4 MΩ were fabricated using a laser-based micropipette puller (P-2000, Sutter Instrument Company, Novato, CA) and filled with an intracellular solution, also containing channel blockers (in mM: 140 CsCl, 2 $MgCl_2$, 10 EGTA, and 10 HEPES). The pH and osmolality of both external and internal solutions were adjusted to 7.2 ± 0.02 and 300 ± 2 mOsm/kg with the addition of CsOH and glucose, respectively. Cell membrane admittance was measured with the patch-clamp technique in the whole-cell mode using a DC voltage ramp with dual-frequency stimulus (Santos-Sacchi et al., 1998) from −0.14 to 0.14 V with a holding potential of 0 volts, and the cell parameters were calculated from the admittance as described earlier (Farrell et al., 2006). The conductance was also determined experimentally with a DC protocol, as described earlier (Rajagopalan et al., 2006). Capacitance curves were fit to a Boltzmann equation, from which charge density (Q_{max}/C_{lin}), voltage at peak capacitance (V_{pkc}), and the unitary change valence or maximum slope of the Boltzmann fit (z) were determined as previously described (Bian et al., 2010; McGuire et al., 2010; Oliver and Fakler, 1999; Rajagopalan et al., 2006).

For isolated OHCs and inducible cells shown in Supplemental Figure 5, membrane capacitance (Cm) was determined using a phase-sensitive detector implemented in PatchMaster (HEKA) as described elsewhere (McGuire et al., 2010). Briefly, an 800-Hz, 10-mV sine wave was applied, and the current response was measured as DC holding potential stepped in 2 mV increments (0.4mV/ms). The phase shift monitored between the output and the input signals allows for determination of the membrane capacitance. Capacitance versus voltage curves were fitted to the two-state C_{sa} model equation (Santos-Sacchi and Navarrete, 2014; Santos-Sacchi and L. Song, 2014):

$$C_m = \frac{Q_{\max}\left(\frac{ze}{kT}\right)}{\exp\left(\frac{ze}{kT}\left(V - V_{pkc}\right)\right) \times \left(1 + \exp\left(\frac{-ze}{kT}\left(V - V_{pkc}\right)\right)\right)^2} + \frac{\Delta C_{SA}}{1 + \left(\exp\left(\frac{-ze}{kT}\left(V - V_{pkc}\right)\right)\right)^{-1}} + C_{lin}$$

where Q_{max} is the maximum nonlinear charge moved, V_{pkc} is the voltage at peak capacitance, V is the membrane potential, z is the valence, e is the electron change, k is Boltzmann's constant, and T is the absolute temperature. The number of motors in the

membrane, N, was defined as $N=Q_{max}/z.e.$ The Student's t-test with Holm adjustment of p-values for multiple comparisons was used to estimate statistical significance. Spearman rank correlations were performed to measure the strength of the relationship between ΔC_{sa} and N.

Results

Charge density increases with time after transient prestin transfection in HEK 293 cells

We measured prestin-associated charge movement as a function of time after HEK 293 cells were transiently transfected with HA-prestin. Transfected cells (visualized by co-expressed GFP epifluorescence) were not visible earlier than 10 hours post-transfection. Prestin was present both within the cell (Supplemental Figure 1A and B) and on the cell surface (Figure 1A) by 10 hours post-transfection and was qualitatively increased by 48 hours. The average percentage of prestin expressed on the cell surface varied substantially between replicates and did not change with increasing time post-transfection (Supplemental Figure 1C). At 10 hours, coincident with the appearance of independently co-expressed GFP epifluorescence, a small non-linear capacitance trace was measured in most patched cells. Calculations of charge density (charge moved per unit membrane capacitance) at each time point reveal a steady increase with the charge density approximately doubling over 48 hours (Spearman rho: 0.68, p-value=$9.708e^{-11}$)(Figure 1B and E). The mean charge density at 36–48 hours was significantly higher than that observed at 10–16 hours ($p<0.005$)(Fig 1B). The voltage at peak capacitance (V_{pkc}) and the maximum slope of the Boltzmann fit (z) were constant over the period of analysis (Figure 1C and D).

Charge density increases with time after induction of prestin expression

To better quantify the relationship between prestin expression and function, we created an inducible prestin-expressing cell line in which prestin expression can be tightly controlled and modulated (see Table 1). Addition of the inducer (Dox) allows expression of prestin-mGFP in these cells, and expression of prestin increased steadily both within the cell (Supplemental Figure 2A and B) and at the cell surface (Figure 2A, top panel) up to 72 hours after induction with 2 μg/ml Dox. The percentage of prestin expressed on the cell surface (surface/total prestin) trended toward increasing with time post-induction, but did not achieve statistical significance (Supplemental Figure 2C). The small variation between replicates in the inducible cell line is consistent with the tightly controlled and reproducible prestin expression (Supplemental Figure 2C versus 1C). Immunodetection of membrane prestin expression by western blotting was evident by 16 hours and was significant by 24 hours post-induction ($p<0.01$) with further significant increases between 24 and 48 hours ($p<0.01$) (Figure 2A, bottom panel). We measured prestin-associated charge movement in these cells at various times post-induction and observed a trend towards increasing charge density from 16 to 56 hours post-induction (Figure 2B). The mean charge density at 56 hours ($p<0.05$) was significantly higher than the mean charge density at 24 hours, reflecting a gradual time-dependent increase. The charge density reached a plateau of approximately 7–10 fC/pF between 56 and 72 hours (Figure 2B). The unitary charge valence (z) had an initial increase between 16 and 24 hours post-induction and an approximately 0.24 overall increase between 16 and 72 hours ($p<0.05$); otherwise, the slope remained constant at the

intermediate time points (Figure 2C). These results indicate a qualitative correlation between membrane prestin levels and charge density (Figure 2D).

Charge density increases as a function of inducer dose

We next determined the optimal concentration of inducer for induction of prestin-associated charge movement by varying the concentrations of Dox, ranging from 0 to 10 μg/ml. Both the intracellular (Supplemental Figure 3A and B) and membrane (Figure 3A, top panel) expression of prestin increased steadily as a function of inducer dose. The percentage of prestin expressed on the cell surface, calculated as surface/total prestin, did not vary significantly with increasing inducer dose (Supplemental Figure 3C). However, membrane prestin expression increased significantly between 0 and 1 μg/ml Dox ($p<0.01$), between 1 and 2 μg/ml Dox ($p<0.05$), and between 2 and 4 μg/ml Dox ($p<0.05$). Although the trend of increasing membrane prestin expression continued up to 6 μg/ml Dox ($p<0.05$), there was no statistical difference in expression at doses of 6 to 10 μg/ml Dox (Figure 3A, bottom panel). Charge density showed an initial increase with 0.5 and 1 μg/ml Dox ($p<0.05$), steadily rose with increasing amounts of inducer until reaching a statistical difference at 6 μg/ml ($p<0.005$, compared to 1 μg/ml), and remained constant at 10–12 fC/pF within statistical margins between 6 and 10 μg/ml (Figure 3B). The unitary charge valence (z) significantly increased by approximately 25% between 0 and 1 μg/ml Dox; however, there were no further increases in z values above 2 μg/ml Dox (Figure 3C). Both membrane prestin expression and average charge density increased in a dose-dependent fashion and reached a plateau at higher concentrations (Figure 3D), indicating that charge movement reaches ‘saturation’ after a certain inducer (approximately 6 μg/ml) concentration.

Membrane prestin levels and charge density gradually decline after removal of Dox

If prestin membrane expression levels are directly correlated with charge density, depletion of prestin from the membrane should decrease this readout. After removing Dox from the cell growth medium to stop induction of prestin expression, we determined the decline in prestin-associated charge movement. Within the first 24 hours after Dox removal, intracellular levels of prestin trended upwards and then decreased steadily (Supplemental Figure 4A and B). Following inducer removal, membrane prestin levels progressively decreased and were significantly depleted by 36 to 48 hours ($p<0.05$; Figure 4A), with a concurrent decrease in charge density of approximately 65% by 48 hours (Figure 4B and D). There were no statistically significant changes in the unitary charge valence (z) after Dox removal (Figure 4C). The half-life of prestin-mGFP on the cell surface is approximately 24 hours following Dox removal (Supplemental Figure 4C). Collectively, these data indicate that the magnitude of charge density is directly dependent on membrane prestin levels.

V_{pkc} is independent of time and inducer dose

To determine whether prestin expression levels in the inducible cell line affects voltage at peak capacitance (V_{pkc}), we compared V_{pkc} at different time-points, at different Dox doses, and after Dox removal. We observed no statistically significant changes in the average V_{pkc} among different treatment groups (Figure 5, A–C). This suggests that the mechanisms controlling the V_{pkc} aspect of prestin-associated charge movement are distinct from those responsible for the increase in charge density.

The inducible cell line closely models ΔC_{sa} values and the estimated number of motors in isolated murine outer hair cells (OHCs)

Comparison of data from our inducible cell line and from isolated murine OHCs using the area motor model yield equivalent values for ΔC_{sa}, the membrane-dependent change in capacitance that results from changes in the surface area, and for the estimated number of motors in the membrane ($N=Qmax/z.e$) (Supplemental Figure 5). ΔC_{sa} correlates strongly with the estimated number of motors in the inducible cell line (Spearman's rho = 0.863158, p=2.2e–16) and in isolated murine OHCs (Spearman's rho = 0.520879, p = 0.05). Further, the resulting normalized ΔC_{sa} obtained from the linear fit of ΔC_{sa} = f(N) for the inducible cell line and OHCs are 260±31 zF and 203±71 zF respectively (slope ± standard error).

Discussion

Many studies investigating prestin-associated charge movement begin with the fundamental assumption that there is a direct relationship between prestin expression (molecular density in the membrane) and charge movement. However, disagreements about the exact timelines of prestin expression and NLC maturation provoke questions about the direct correlation between membrane levels of prestin and prestin-associated charge movement. Whereas Belyantseva and colleagues reported that prestin expression coincides with the development of electromotility in the rat OHCs (Belyantseva et al., 2000), a study in mice indicates that the magnitude of NLC continues to increase days after prestin levels plateau during OHC development (Abe et al., 2007). The conclusions of the latter study appear to contradict conventional assumptions that the amount of charge moved depends solely on the number of prestin molecules in the membrane and point to the possibility that additional mechanism(s) may regulate prestin and OHC functional maturation.

We specifically investigated the correlation between prestin expression and function using a cell line with inducible prestin expression, which facilitates modulation of overall prestin expression and evaluation of prestin membrane and cellular populations under controlled conditions. By using different inducer doses and induction times, we generated tightly controlled dose- and time-dependent membrane expression profiles of prestin. We observed a specific correlation between prestin expression and charge density up to a saturation point, beyond which additional prestin expression no longer increases charge density (Figures 2 and 3, panels A–B, D). Conversely, when prestin-associated charge movement is measured following inducer removal, charge density progressively decreases as membrane prestin levels decline (Figure 4A–B, D). The correlation between time-dependent expression profiles of prestin and charge density (Figure 2A–B, D) is consistent with recent findings in a tetracycline-inducible prestin-expressing cell line (Bian et al., 2013; 2010). Notably, our analysis further characterizes the relationship between prestin membrane expression and function in the contexts of dose- and time-dependence of induction, as well as the half-life of prestin and its associated charge movement upon removal of the inducer, with increased statistical detail and stringency. In addition, the constant expression of the general membrane protein (EGFR) clarifies interpretation of the prestin surface expression findings, which support the conventional assumption that there is indeed a direct quantitative relationship between the amount of prestin in the membrane and charge density over a large range of

prestin expression levels (Figures 2D, 3D, and 4D). Comparison of data from our inducible cell line and from isolated murine OHCs using the area motor model yield similar values for ΔC_{sa}, the membrane-dependent change in capacitance that results from changes in the surface area, and for the estimated number of motors in the membrane ($N=Qmax/z.e$) (Supplemental Figure 5). We can conclude that the motor behavior of prestin is comparable in the inducible cell line and in murine OHCs, yielding a similar impact on the membrane capacitance upon activation. Interestingly, prestin expression can itself be regulated by OHC stimulation, suggesting the presence of a local feedback mechanism (Y. Song et al., 2015).

The plateau in charge density may be due to one or more factors. First, it is likely that at high expression levels, there is continuous prestin recycling in and out of the membrane. Although cellular prestin levels continue to increase, the functional membrane population remains fairly constant, which is consistent with the absence of statistically significant changes in the percentage of total prestin expressed on the cell surface (Supplemental Figures 2C and 3C). Indeed, we have previously demonstrated that membrane prestin is under active regulation by endocytic vesicle trafficking (Rajagopalan et al., 2010), and others have found that prestin's interaction with these vesicles and proper targeting to the OHC basolateral membrane require tyrosine motifs (Y. Zhang et al., 2015). Alternatively, increased prestin density in the membrane may hinder the conformational flexibility required for optimal function. We have previously demonstrated that steric hindrance can ablate or modify prestin function (Rajagopalan et al., 2006). Another possibility is that the availability of anions or cofactor(s) required for prestin function becomes limiting beyond a certain point.

We further evaluated the Boltzmann characteristics of NLC by examining the unitary charge valence (z), which estimates the amount of charge carried by an individual motor. Our analysis of z with time after induction showed a statistically significant increase in z values between 16 and 24 hrs and a subsequent plateau through 72 hours (Figure 2C). Bian et al. (2010) found a similar pattern of initial increase followed by a plateau, though the specific timing of the increase differed—a gradual increase in our system compared to a rapid increase in theirs—possibly due to different induction characteristics of the inducible systems. Our system features a gradual increase and overall lower levels of prestin whereas the Bian et al. inducible system rapidly overexpressed prestin at levels even higher than transiently transfected HEK cells (Bian et al., 2013; 2010). Bian et al. related their findings to different ratios between upper and lower prestin monomer species observed in their biochemical analysis of surface prestin expression (Bian et al., 2010). We did not observe this effect under any of our experimental conditions, which may be due to our gradual and lower levels of prestin expression.

In addition to the temporal relationship between surface expression and unitary charge valence, we showed a significant increase in z values from 0 to 2 μg/ml Dox and a plateau between 2 and 10 μg/ml Dox (Figure 3C). Collectively, our results suggest that increasing doses of inducer initially increase prestin membrane expression, unitary charge valence, and charge density with unitary charge valence saturating at 2 μg/ml Dox and prestin membrane expression and charge density reaching a plateau at 6 μg/ml Dox. When the inducer was removed, the unitary charge valence remained unchanged (Figure 4C), indicating that once

the unitary charge valence reaches a maximum value (Figure 3C), decreasing prestin membrane expression and charge density does not alter the charge carried by an individual motor in the membrane.

Another Boltzmann characteristic of NLC maturation is the voltage at peak capacitance (V_{pkc}), which reflects the voltage dependence of the motor protein prestin. During development, there is a significant shift of V_{pkc} from hyperpolarized to depolarized voltages characteristic of mature OHCs (Oliver and Fakler, 1999). The V_{pkc} shift appears to coincide with the increase in charge density in rat OHCs (Belyantseva et al., 2000). In mice, V_{pkc} values appear to reach a steady state after postnatal day 14, which occurs after the plateau in prestin levels but before development of the full magnitude of NLC (Abe et al., 2007). The mechanism responsible for the shift in V_{pkc} is unknown, and it is unclear whether the position of V_{pkc} directly correlates with prestin expression and/or the increase in charge density.

While charge density shows a clear relationship to prestin expression, there is no correlation between prestin membrane expression and the voltage at peak capacitance (V_{pkc}). In our doxycycline-inducible cell line expressing prestin-GFP, V_{pkc} remains essentially unchanged in both transiently transfected cells and across all inducer doses and induction times in the inducible cell line (Figures 1B and 5). Bian et al. (2010) reported a trend towards more depolarized potentials with time after induction that was not statistically significant. The absence of statistically significant changes in V_{pkc} suggests that different mechanisms are responsible for the charge density and V_{pkc} aspects of prestin-associated charge movement. Several other factors may play a role in the full development of OHC electromotility and the shift of V_{pkc} from hyperpolarized voltages to depolarized values. Intracellular chloride levels play a major role in prestin function, regulating the magnitude of charge movement (Oliver et al., 2001; Santos-Sacchi et al., 2006; Santos-Sacchi and L. Song, 2014; L. Song and Santos-Sacchi, 2010). The role of anion levels in regulating the voltage at peak capacitance and the mechanisms by which these anion levels change during development are not well understood, although mutations of charged residues that presumably interact with anions shift V_{pkc} significantly (Rajagopalan et al., 2006).

Membrane composition, which may change during development, is another factor that may regulate prestin function. Several studies have reported alterations in OHC lateral wall membrane composition, specifically cholesterol, during development (Nguyen and Brownell, 1998; Oghalai et al., 1998; Rajagopalan et al., 2007; Sturm et al., 2006). The hyperpolarizing effect of high membrane cholesterol coupled with the finding that cholesterol levels decrease in the OHC lateral wall during development, suggests that membrane cholesterol levels may play a key regulatory role in NLC maturation. Our previous studies demonstrated that changes in membrane composition can dramatically and reversibly affect V_{pkc} (Rajagopalan et al., 2007; Sfondouris et al., 2008). Changes in cholesterol can alter OHC membrane lipid fluidity, which may affect prestin function (Organ and Raphael, 2009). A recent study using a prestin-YFP knockin mouse model showed that disrupting lateral wall membrane structure with a cholesterol-depleting agent and salicylate increased lateral mobility of prestin, which would have functional consequences for both normal development and disorders of cholesterol metabolism (Yamashita et al., 2015).

Increased expression of other OHC membrane, cytoskeletal, and prestin-associated proteins, may provide additional maturation mechanisms for the full development of adult OHC electromotility, either by direct association with prestin or by altering membrane material properties such as stiffness and tension (Jensen-Smith and Hallworth, 2007; Santos-Sacchi et al., 1998; R. Zhang et al., 2007).

In conclusion, our data suggest that the generation of prestin-associated charge movement involves two distinct aspects. Increased charge density is directly related to the increase in membrane prestin expression. On the other hand, the V_{pkc} shift is likely to be affected by other processes, such as altered membrane composition and material properties, which deserve further study. Our inducible cell line, which closely mimics the behavior of prestin in murine OHCs, will be a valuable tool for future studies.

Supplementary Material

Refer to Web version on PubMed Central for supplementary material.

Acknowledgments

This work was funded by DC00354 (NIDCD; to WEB and FAP), DC008134 and DC009622 (NIDCD; to FAP), W. M. Keck Center for Interdisciplinary Bioscience Training (LR), NIH/NIA 5T32 Training Grant AG00183 (MLS, 2010–2012) and NIDCD/NIH NRSA award number F31DC012503 (MLS, 2012–2015). The authors wish to thank Sarah Pfannenschmidt for technical assistance with the quantification of prestin cell surface expression and Dr. Henry Pownall for comments that greatly improved an earlier version of this manuscript.

Abbreviations

OHC	outer hair cell
NLC	non-linear capacitance
Dox	doxycycline
Tet	tetracycline

References

Abe T, Kakehata S, Kitani R, Maruya S, Navaratnam D, Santos-Sacchi J, Shinkawa H. Developmental expression of the outer hair cell motor prestin in the mouse. J Membr Biol. 2007; 215:49–56. DOI: 10.1007/s00232-007-9004-5 [PubMed: 17415610]

Adler HJ, Belyantseva IA, Merritt RCJ, Frolenkov GI, Dougherty GW, Kachar B. Expression of prestin, a membrane motor protein, in the mammalian auditory and vestibular periphery. Hear Res. 2003; 184:27–40. [PubMed: 14553901]

Ashmore J. Cochlear outer hair cell motility. Physiol Rev. 2008; 88:173–210. DOI: 10.1152/physrev.00044.2006 [PubMed: 18195086]

Ashmore JF. A fast motile response in guinea-pig outer hair cells: the cellular basis of the cochlear amplifier. J Physiol (Lond). 1987; 388:323–347. DOI: 10.1111/(ISSN)1469-7793 [PubMed: 3656195]

Ashmore JF. Neurosci Res Suppl. 1990; 12:S39–50. [PubMed: 2243636]

Belyantseva IA, Adler HJ, Curi R, Frolenkov GI, Kachar B. Expression and localization of prestin and the sugar transporter GLUT-5 during development of electromotility in cochlear outer hair cells. J Neurosci. 2000; 20:RC116. [PubMed: 11125015]

Bian S, Koo BW, Kelleher S, Santos-Sacchi J, Navaratnam DS. A highly expressing Tet-inducible cell line recapitulates in situ developmental changes in prestin's Boltzmann characteristics and reveals early maturational events. Am J Physiol, Cell Physiol. 2010; 299:C828–35. DOI: 10.1152/ajpcell.00182.2010 [PubMed: 20631244]

Bian S, Navaratnam D, Santos-Sacchi J. Real time measures of prestin charge and fluorescence during plasma membrane trafficking reveal sub-tetrameric activity. PLoS ONE. 2013; 8:e66078.doi: 10.1371/journal.pone.0066078 [PubMed: 23762468]

Brownell, WE. The piezoelectric hair cell. In: Eatock, RA., editor. Vertebrate Hair Cells. Springer; New York: 2006. p. 313-347.

Brownell WE, Bader CR, Bertrand D, de Ribaupierre Y. Evoked mechanical responses of isolated cochlear outer hair cells. Science. 1985; 227:194–196. [PubMed: 3966153]

Dallos P, Wu X, Cheatham MA, Gao J, Zheng J, Anderson CT, Jia S, Wang X, Cheng WH, Sengupta S, He DZ, Zuo J. Prestin-based outer hair cell motility is necessary for mammalian cochlear amplification. Neuron. 2008; 58:333–339. DOI: 10.1016/j.neuron.2008.02.028 [PubMed: 18466744]

Farrell B, Do Shope C, Brownell WE. Voltage-dependent capacitance of human embryonic kidney cells. Phys Rev E Stat Nonlin Soft Matter Phys. 2006; 73:041930. [PubMed: 16711859]

He DZZ, Jia S, Sato T, Zuo J, Andrade LR, Riordan GP, Kachar B. Changes in plasma membrane structure and electromotile properties in prestin deficient outer hair cells. Cytoskeleton. 2010; 67:43–55. DOI: 10.1002/cm.20423 [PubMed: 20169529]

Holm S. A Simple Sequentially Rejective Multiple Test Procedure. Scandinavian Journal of Statistics. 1979; 6:65–70.

Jensen-Smith H, Hallworth R. Lateral wall protein content mediates alterations in cochlear outer hair cell mechanics before and after hearing onset. Cell Motil Cytoskeleton. 2007; 64:705–717. [PubMed: 17615570]

Kalinec F, Holley MC, Iwasa KH, Lim DJ, Kachar B. A membrane-based force generation mechanism in auditory sensory cells. Proc Natl Acad Sci USA. 1992; 89:8671–8675. [PubMed: 1528879]

Liberman MC, Gao J, He DZ, Wu X, Jia S, Zuo J. Prestin is required for electromotility of the outer hair cell and for the cochlear amplifier. Nature. 2002; 419:300–304. DOI: 10.1038/nature01059 [PubMed: 12239568]

Ludwig J, Oliver D, Frank G, Klocker N, Gummer AW, Fakler B. Reciprocal electromechanical properties of rat prestin: the motor molecule from rat outer hair cells. Proc Natl Acad Sci USA. 2001; 98:4178–4183. DOI: 10.1073/pnas.071613498 [PubMed: 11274441]

Mahendrasingam S, Beurg M, Fettiplace R, Hackney CM. The ultrastructural distribution of prestin in outer hair cells: a post-embedding immunogold investigation of low-frequency and high-frequency regions of the rat cochlea. European Journal of Neuroscience. 2010; 31:1595–1605. DOI: 10.1111/j.1460-9568.2010.07182.x [PubMed: 20525072]

McGuire RM, Liu H, Pereira FA, Raphael RM. Cysteine mutagenesis reveals transmembrane residues associated with charge translocation in prestin. J Biol Chem. 2010; 285:3103–3113. DOI: 10.1074/jbc.M109.053249 [PubMed: 19926791]

Muallem D, Ashmore J. An anion antiporter model of prestin, the outer hair cell motor protein. Biophysj. 2006; 90:4035–4045. DOI: 10.1529/biophysj.105.073254

Nguyen TV, Brownell WE. Contribution of membrane cholesterol to outer hair cell lateral wall stiffness. Otolaryngol Head Neck Surg. 1998; 119:14–20. [PubMed: 9674509]

Oghalai JS, Patel AA, Nakagawa T, Brownell WE. Fluorescence-imaged microdeformation of the outer hair cell lateral wall. J Neurosci. 1998; 18:48–58. [PubMed: 9412485]

Oliver D, Fakler B. Expression density and functional characteristics of the outer hair cell motor protein are regulated during postnatal development in rat. J Physiol (Lond). 1999; 519(Pt 3):791–800. [PubMed: 10457091]

Oliver D, He DZ, Klocker N, Ludwig J, Schulte U, Waldegger S, Ruppersberg JP, Dallos P, Fakler B. Intracellular anions as the voltage sensor of prestin, the outer hair cell motor protein. Science. 2001; 292:2340–2343. DOI: 10.1126/science.1060939 [PubMed: 11423665]

Organ LE, Raphael RM. Lipid lateral mobility in cochlear outer hair cells: regional differences and regulation by cholesterol. JARO. 2009; 10:383–396. DOI: 10.1007/s10162-009-0171-1 [PubMed: 19517190]

Rajagopalan L, Greeson JN, Xia A, Liu H, Sturm A, Raphael RM, Davidson AL, Oghalai JS, Pereira FA, Brownell WE. Tuning of the outer hair cell motor by membrane cholesterol. J Biol Chem. 2007; 282:36659–36670. [PubMed: 17933870]

Rajagopalan L, Organ-Darling LE, Liu H, Davidson AL, Raphael RM, Brownell WE, Pereira FA. Glycosylation regulates prestin cellular activity. JARO. 2010; 11:39–51. DOI: 10.1007/s10162-009-0196-5 [PubMed: 19898896]

Rajagopalan L, Patel N, Madabushi S, Goddard JA, Anjan V, Lin F, Shope C, Farrell B, Lichtarge O, Davidson AL, Brownell WE, Pereira FA. Essential helix interactions in the anion transporter domain of prestin revealed by evolutionary trace analysis. J Neurosci. 2006; 26:12727–12734. DOI: 10.1523/JNEUROSCI.2734-06.2006 [PubMed: 17151276]

Rybalchenko V, Santos-Sacchi J. Anion control of voltage sensing by the motor protein prestin in outer hair cells. Biophys J. 2008; 95:4439–4447. DOI: 10.1529/biophysj.108.134197 [PubMed: 18658219]

Rybalchenko V, Santos-Sacchi J. Cl− flux through a non-selective, stretch-sensitive conductance influences the outer hair cell motor of the guinea-pig. J Physiol (Lond). 2003; 547:873–891. DOI: 10.1113/jphysiol.2002.036434 [PubMed: 12562920]

Santos-Sacchi J. Reversible inhibition of voltage-dependent outer hair cell motility and capacitance. J Neurosci. 1991a; 11:3096–3110. [PubMed: 1941076]

Santos-Sacchi J. Isolated supporting cells from the organ of Corti: some whole cell electrical characteristics and estimates of gap junctional conductance. Hearing Research. 1991b; 52:89–98. [PubMed: 2061216]

Santos-Sacchi J, Kakehata S, Takahashi S. Effects of membrane potential on the voltage dependence of motility-related charge in outer hair cells of the guinea-pig. J Physiol. 1998; 510:225–235. [PubMed: 9625879]

Santos-Sacchi J, Navarrete E. Voltage-dependent changes in specific membrane capacitance caused by prestin, the outer hair cell lateral membrane motor. Pflügers Arch - Eur J Physiol. 2014; 444:99–106. DOI: 10.1007/s00424-002-0804-2 [PubMed: 11976921]

Santos-Sacchi J, Song L, Zheng J, Nuttall AL. Control of Mammalian Cochlear Amplification by Chloride Anions. The Journal of neuroscience : the official journal of the Society for Neuroscience. 2006; 26:3992–3998. DOI: 10.1523/JNEUROSCI.4548-05.2006 [PubMed: 16611815]

Santos-Sacchi J, Song L. Chloride and salicylate influence prestin-dependent specific membrane capacitance: support for the area motor model. J Biol Chem. 2014; 289:10823–10830. DOI: 10.1074/jbc.M114.549329 [PubMed: 24554714]

Schaechinger TJ, Oliver D. Nonmammalian orthologs of prestin (SLC26A5) are electrogenic divalent/chloride anion exchangers. Proc Natl Acad Sci USA. 2007; 104:7693–7698. DOI: 10.1073/pnas.0608583104 [PubMed: 17442754]

Sfondouris J, Rajagopalan L, Pereira FA, Brownell WE. Membrane composition modulates prestin-associated charge movement. J Biol Chem. 2008; 283:22473–22481. [PubMed: 18567583]

Song L, Santos-Sacchi J. Conformational State-Dependent Anion Binding in Prestin: Evidence for Allosteric Modulation. Biophysj. 2010; 98:371–376. DOI: 10.1016/j.bpj.2009.10.027

Song Y, Xia A, Lee HY, Wang R, Ricci AJ, Oghalai JS. Activity-dependent regulation of prestin expression in mouse outer hair cells. J Neurophysiol. 2015; 113:3531–3542. DOI: 10.1152/jn.00869.2014 [PubMed: 25810486]

Sturm AK, Rajagopalan L, Yoo D, Brownell WE, Pereira FA. Expression and subcellular localization of prestin in cultured cells. Otolaryngol Head Neck Surg. 2006; 136:434–439. [PubMed: 17321873]

Xia A, Wooltorton JR, Palmer DJ, Ng P, Pereira FA, Eatock RA, Oghalai JS. Functional prestin transduction of immature outer hair cells from normal and prestin-null mice. J Assoc Res Otolaryngol. 2008; 9:307–320. DOI: 10.1007/s10162-008-0121-3 [PubMed: 18506528]

Yamashita T, Hakizimana P, Wu S, Hassan A, Jacob S, Temirov J, Fang J, Mellado-Lagarde M, Gursky R, Horner L, Leibiger B, Leijon S, Centonze VE, Berggren PO, Frase S, Auer M, Brownell WE, Fridberger A, Zuo J. Outer Hair Cell Lateral Wall Structure Constrains the Mobility of Plasma Membrane Proteins. PLoS Genet. 2015; 11:e1005500.doi: 10.1371/journal.pgen.1005500 [PubMed: 26352669]

Yu N, Zhu ML, Zhao HB. Prestin is expressed on the whole outer hair cell basolateral surface. Brain Res. 2006; 1095:51–58. [PubMed: 16709400]

Zhang R, Qian F, Rajagopalan L, Pereira FA, Brownell WE, Anvari B. Prestin modulates mechanics and electromechanical force of the plasma membrane. Biophys J. 2007; 93:L07–9. [PubMed: 17468166]

Zhang Y, Moeini-Naghani I, Bai J, Santos-Sacchi J, Navaratnam DS. Tyrosine motifs are required for prestin basolateral membrane targeting. Biol Open. 2015; 4:197–205. DOI: 10.1242/bio.201410629 [PubMed: 25596279]

Zheng J, Shen W, He DZ, Long KB, Madison LD, Dallos P. Prestin is the motor protein of cochlear outer hair cells. Nature. 2000; 405:149–155. DOI: 10.1038/35012009 [PubMed: 10821263]

Research Highlights

- Determined contribution of membrane prestin levels to generation of NLC using inducible system.
- Charge density directly correlates with membrane prestin levels.
- Membrane prestin levels do not significantly affect voltage at peak capacitance.
- Charge density and voltage at peak capacitance may involve distinct processes.

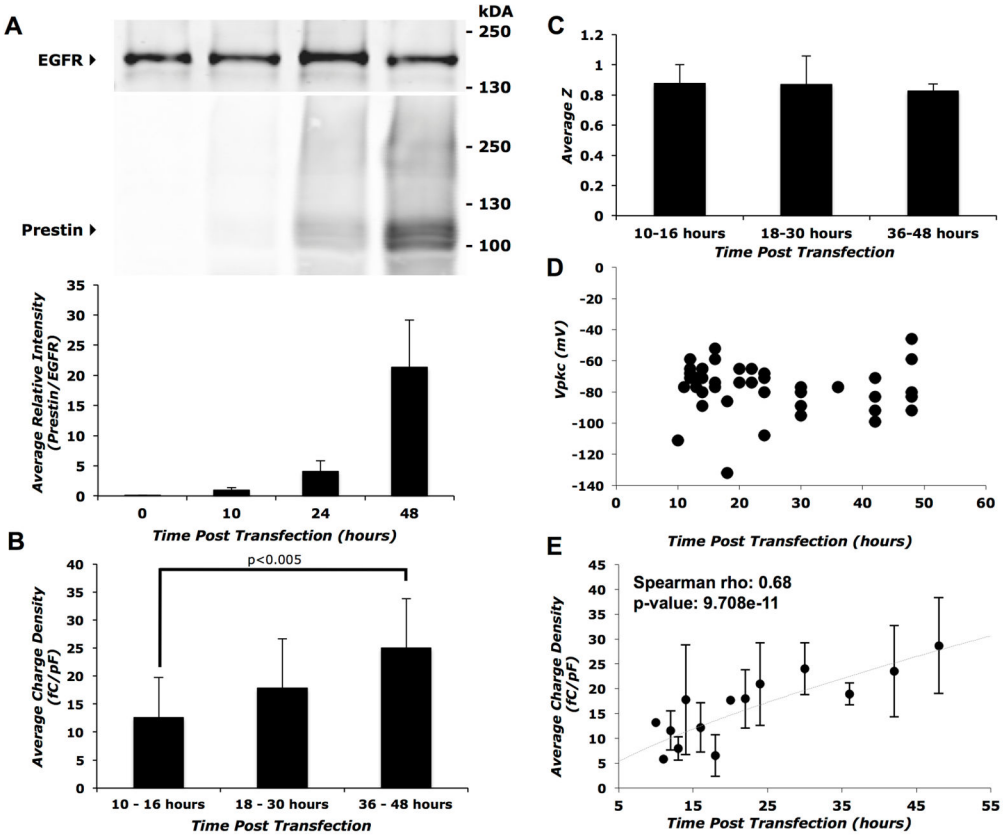

Figure 1. Time-course of prestin expression and function in transiently transfected HEK 293 cells

A) Top panel: representative western blot of biotinylated cell surface proteins showing a gradual increase in prestin expression with time after transient transfection with HA-prestin. Bottom panel: average band intensity of prestin relative to EGFR calculated from three independent western blots as a function of time post-transfection. B) Average charge density for three groups of time points (10–16 hrs, 18–30 hrs, and 36–48 hrs). The 36–48 hour group showed a statistically significant increase ($p<0.005$) in comparison with the 10–16 hour group using the Student's t-test with Holm adjustment of p-values for multiple comparisons. Sample size, n = 18, 14 and 11 for the 10–16, 18–30 and the 36–48 hour groups respectively. C) Average z values of prestin transfected cells at different time points post-transfection. There were no statistically significant differences in the unitary charge valence (z) with time post-transfection. Sample sizes were the same as in (B). D) Individual data points of V_{pkc} at time-points post transfection. The V_{pkc} remains fairly constant between 10 and 48 hours. Sample sizes were the same as in (B). E) Average charge densities of prestin transfected cells at different time-points post-transfection. Error bars represent standard deviation in all panels. Spearman *rho* correlation coefficient and associated p-value were calculated to estimate correlation significance.

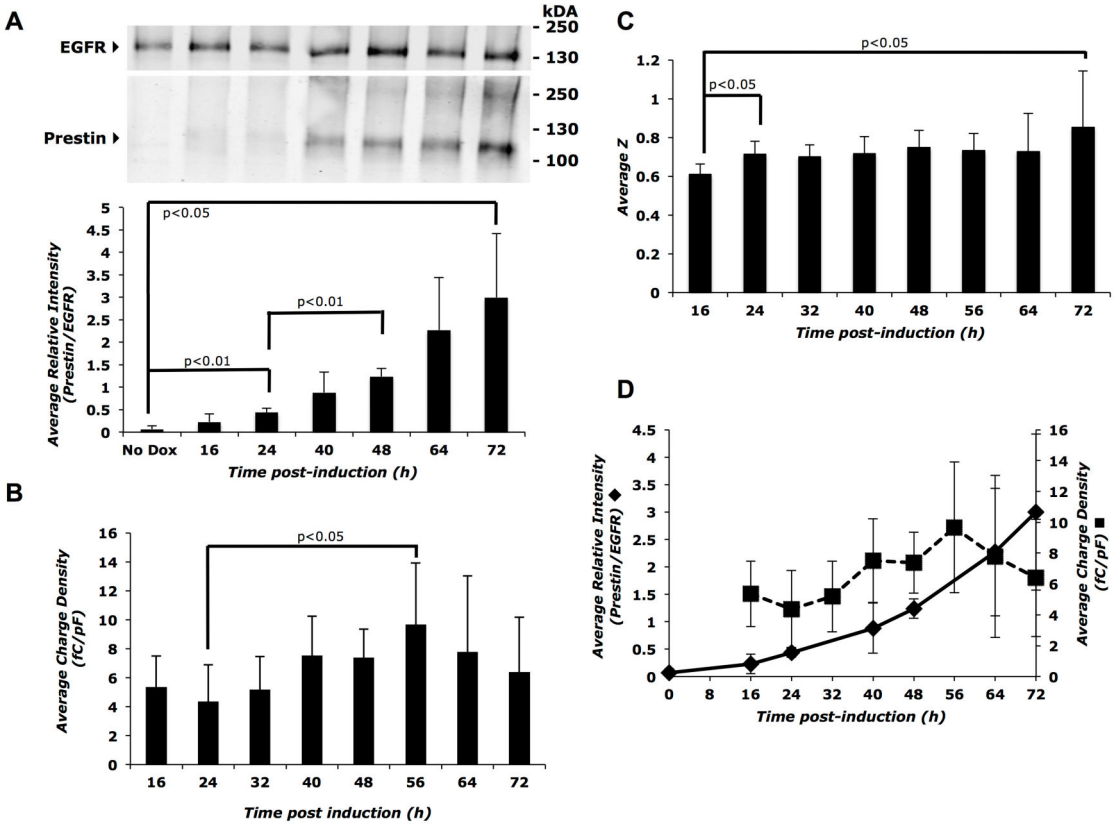

Figure 2. Membrane prestin expression and charge density increase with time after induction in the Prestin-mGFP Tet-On inducible cell line

A) Top panel: representative Western blot of biotinylated cell surface proteins showing a gradual increase in prestin expression after addition of the inducer, 2 μg/ml Dox. Control plates were grown for 72 hours in the absence of Dox. Bottom panel: average band intensity of prestin relative to EGFR calculated from three independent western blots as a function of time post-induction. B) A corresponding increase is seen in the average charge density up to 56 hours post induction, reaching a plateau at further time points. Dox was added again to the cells at 48 hours to continue robust prestin expression. Sample size, n = 6 to 9 cells for each time point. C) Average z values increase between 16–24 hours and then remain steady through 72 hours post-induction. Sample sizes were the same as in (B). D) Dual axis plot showing parallel increases in membrane prestin expression (primary y-axis) and average charge density (secondary y-axis) as a function of time post-induction. Error bars represent standard deviation in all panels. The Student's t-test with Holm adjustment of p-values for multiple comparisons was used to estimate statistical significance; resulting p-values are indicated in each panel.

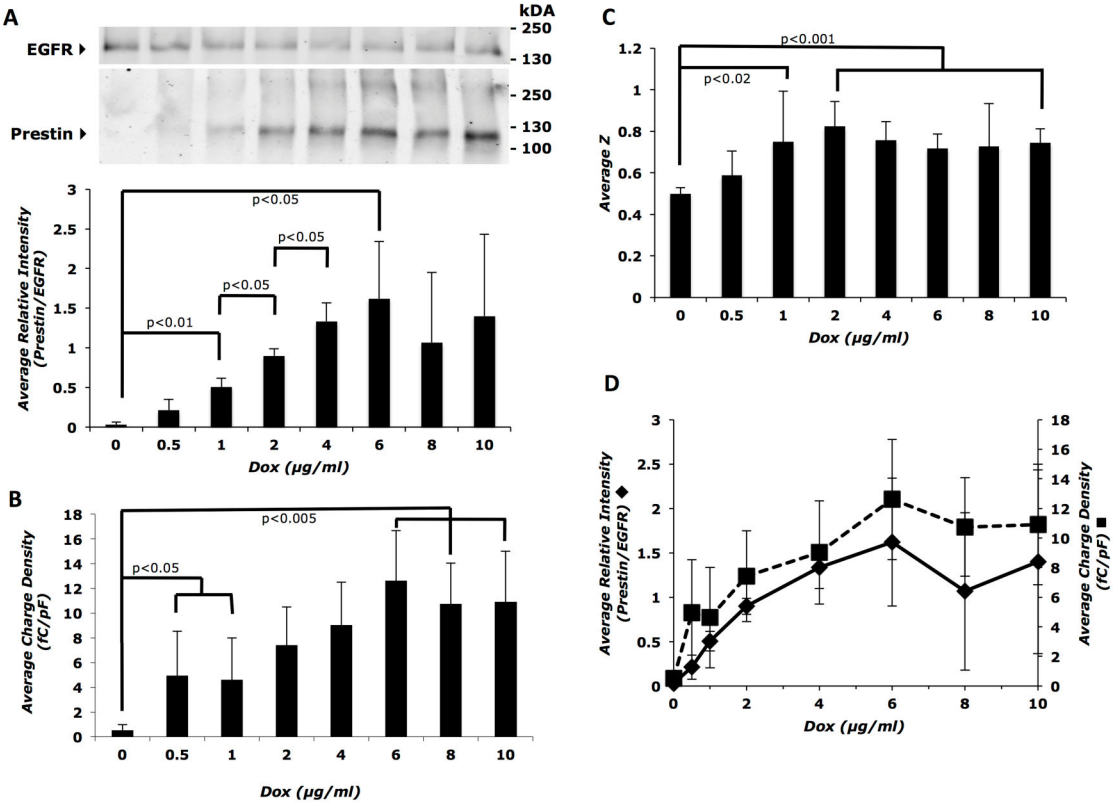

Figure 3. Membrane prestin expression and charge density increase as a function of inducer (Dox) dose

A) Top panel: representative western blot of biotinylated cell surface proteins showing a gradual increase in prestin expression with inducer dose, reaching a maximum by 6 µg/ml Dox. Bottom panel: average band intensity of prestin relative to EGFR calculated from three independent western blots as a function of inducer dose. B) Average charge density at each inducer dose (n = 8 to 12 cells for each Dox dose) shows a corresponding increase that also reaches a plateau at 6 µg/ml Dox. C) Average z values increase with inducer dose up to 2 µg/ml and then remain constant. Sample sizes were the same as in (B). D) Dual axis plot showing parallel increases in membrane prestin expression (primary y-axis) and average charge density (secondary y-axis) as a function of inducer (Dox) dose. Error bars represent standard deviation in all panels. The Student's t-test with Holm adjustment of p-values for multiple comparisons was used to estimate statistical significance; resulting p-values are indicated in each panel.

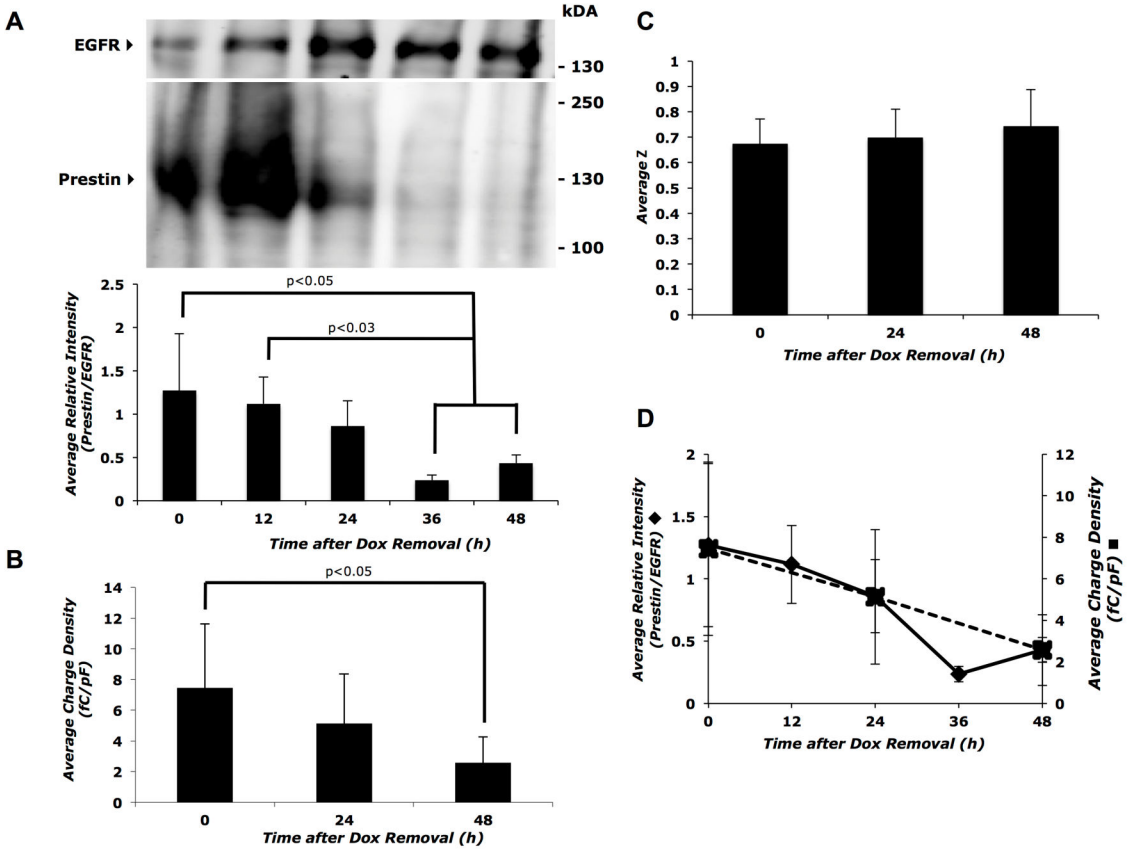

Figure 4. Decline in prestin expression and function after Dox removal

A) Top panel: representative western blot of biotinylated cell surface proteins showing the progressive decrease in prestin expression following the removal of Dox from the cell culture media. Bottom panel: average band intensity of prestin relative to EGFR calculated from three independent Western blots as a function of time after Dox removal. B) A corresponding decrease in charge density is seen up to 48 hours after Dox removal (n= 8 to 9 cells per time point). C) Average z values did not change with time after Dox removal. Sample sizes were the same as in (B). D) Dual axis plot showing parallel decreases in membrane prestin expression (primary y-axis) and average charge density (secondary y-axis) with time after Dox removal. Error bars represent standard deviation in all panels. The Student's t-test with Holm adjustment of p-values for multiple comparisons was used to estimate statistical significance; resulting p-values are indicated in each panel.

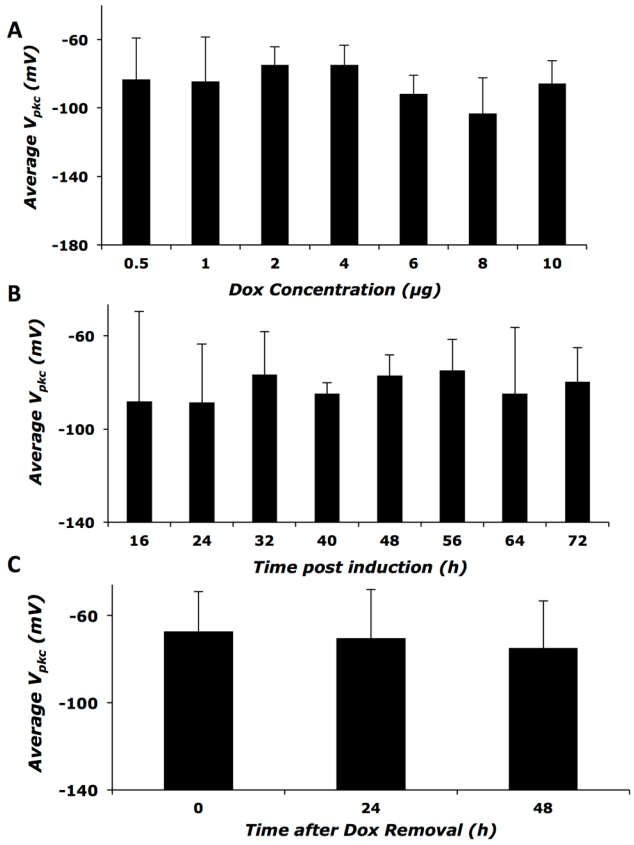

Figure 5. V_{pkc} shows no change as a function of prestin expression

A) Average Vpkc of cells induced with various doses of Dox. B) Average V_{pkc} as a function of time after induction. C) Average V_{pkc} at 0 to 48 hours after removal of Dox. Error bars represent standard deviation in all panels. No statistically significant difference is seen among any of the treatment groups. Sample sizes are the same as mentioned earlier for the different treatments.

Table 1

Parameters of prestin-associated charge movement from cell lines with transient or inducible prestin expression and from murine OHCs.

HEK293 cells	***Charge Density* (fC/pF)**	**V_{pkc} (mV)**	***z***	***n***
Transient transfection	28.7 ± 9.6	−72 ± 18.9	0.8 ± 0.04	5
Dox-Induced (6 μg/ml)	12.6 ± 4.1	−91.8 ± 10.9	0.72 ± 0.07	8
Dox-Induced (2 μg/ml)	7.4 ± 3.1	−74.7 ± 10.4	0.82 ± 0.12	8
Murine OHCs	118.06 ± 22.87	−53.81 ± 14.37	0.79 ± 0.06	21

Values are reported as means ± standard deviation of prestin-associated charge movement parameters at steady-state of prestin expression post-treatment: transiently transfected HA-prestin in HEK 293 cells and in 6 μg/ml or 2 μg/ml Dox-induced prestin-GFP in HEK 293 cells at 48hrs. Isolated murine OHCs are shown for comparison. Charge density varies with time after transfection, as well as with time after induction and inducer dose. The inducible cell line provides a tightly controlled expression of prestin function as evidenced by the small standard deviations. V_{pkc} and z values do not differ between the transiently transfected cell line, the inducible cell line after induction, and murine OHCs, respectively.